Langevin simulations of a long-range electron-phonon model

G. G. Batrouni and Richard T. Scalettar

Phys. Rev. B **99**, 035114 — Published 8 January 2019

DOI: 10.1103/PhysRevB.99.035114

Langevin Simulations of a Long Range Electron Phonon Model

G. G. Batrouni[1,2,3,4,5] and Richard T. Scalettar[6]

[1] *Université Côte d'Azur, INPHYNI, CNRS, 0600 Nice, France*
[2] *MajuLab, CNRS-UCA-SU-NUS-NTU International Joint Research Unit, 117542 Singapore*
[3] *Centre for Quantum Technologies, National University of Singapore, 2 Science Drive 3, 117542 Singapore*
[4] *Department of Physics, National University of Singapore, 2 Science Drive 3, 117542 Singapore*
[5] *Beijing Computational Science Research Center, Beijing 100193, China*
[6] *Department of Physics, University of California, Davis, California 95616, USA*

We present a Quantum Monte Carlo (QMC) study, based on the Langevin equation, of a Hamiltonian describing electrons coupled to phonon degrees of freedom. The bosonic part of the action helps control the variation of the field in imaginary time. As a consequence, the iterative conjugate gradient solution of the fermionic action, which depends on the boson coordinates, converges more rapidly than in the case of electron-electron interactions, such as the Hubbard Hamiltonian. Fourier Acceleration is shown to be a crucial ingredient in reducing the equilibration and autocorrelation times. After describing and benchmarking the method, we present results for the phase diagram focusing on the range of the electron-phonon interaction. We delineate the regions of charge density wave formation from those in which the fermion density is inhomogeneous, caused by phase separation. We show that the Langevin approach is more efficient than the Determinant QMC method for lattice sizes $N \gtrsim 8 \times 8$ and that it therefore opens a potential path to problems including, for example, charge order in the 3D Holstein model.

PACS numbers: 71.10.Fd, 74.20.Rp, 74.70.Xa, 75.40.Mg

I. INTRODUCTION

Quantum Monte Carlo (QMC) constitutes one of the most powerful non-perturbative approaches to interacting fermion Hamiltonians. Its applications have led to insight into both renormalized single particle properties at low density, and also to many-body phase transitions in systems ranging from high energy, to nuclear, to condensed matter physics. Nevertheless, fermion QMC suffers from several serious limitations: (i) Algorithms generally scale as the cube of the number of particles or sites, a consequence of the evaluation of the determinants arising when the fermionic degrees of freedom are integrated out. (ii) Depending on the model and on the parameter regime, long autocorrelation times can also challenge the calculations. Finally, (iii) the fermion sign problem remains the most restrictive bottleneck in the field.

Considerable progress has been made in addressing (i) in the lattice gauge theory (LGT) community, *e.g.* with linear scaling methods for the fermion determinant evaluation. However, these techniques have proven surprisingly difficult to carry over into condensed matter (CM) and specifically to the Hubbard model[1–5]. The general belief is that the difficulty arises from two related problems: the high degree of anisotropy between imaginary time (β) and the spatial dimensions present in CM problems, as opposed to the relativistic LGT case, and the much more rapid variation of the Hubbard-Stratonovich field configurations in the imaginary time direction which gives rise to less well-conditioned matrices. The eigenvalue spread in CM problems leads to large conjugate gradient iteration counts, and, indeed, often, to a complete absence of convergence of iterative matrix inversion solvers.

In this paper we explore the application of linear scaling QMC methods to electron-phonon Hamiltonians. We are motivated by the fact that, in such models, the kinetic energy terms $\sum_i \hat{p}_i^2/2$ in the oscillator Hamiltonian smooth the imaginary time variation of the phonon field. As a consequence, the condition number of the fermion determinants is likely to be improved relative to that which arises in the Hubbard model, where the Hubbard-Stratonovich field has no similar dynamics. It is for the latter case that most of the linear scaling methods have previously been tested[1–4] and shown to be effective only in a limited parameter regime of weak coupling and/or relatively high temperature.

The successful application of Langevin methods to electron-phonon models would be a considerable step forward, since their physics holds significant intrinsic interest. Early QMC work focused on the dilute limit. As an electron moves through a material, the polarization of the underlying medium causes a cloud of phonons to follow. Simulations studied the resulting "single electron polaron", identifying its size and effective mass as functions of the electron-phonon coupling and phonon frequency[6–14]. If the interaction λ is sufficiently large, two polarons can pair with a bipolaron size and dispersion which depend on λ[15].

Meanwhile, as the density increases, QMC has explored how local up and down spin pairs, which form due the effective interaction mediated by the lattice distortion, can arrange themselves spatially into charge density wave (CDW) patterns, especially on bipartite lattices[16–18]. The critical temperatures of transitions to long range order phases have been evaluated[19,22]. These CDW patterns typically induce insulating behavior, and

compete with superconducting phases which can also occur if the pairs become phase coherent across the lattice[16,22].

In the remainder of this paper, Sec. 2 will describe the specific Hamiltonian to be studied, its experimental motivation, and the details of the Langevin method. Section 3 contains benchmarks of our results and comparisons with other methods. Section 4 describes results for the low temperature ordered phases of the Hamiltonian, and Sec. 5 presents some concluding remarks.

II. MODEL AND METHODS

We will study the properties of a two-dimensional system governed by the Hamiltonian,

$$\hat{H} = \hat{H}^0_{\rm el} + \hat{H}^0_{\rm ph} + \hat{V}_{\rm el-ph}, \tag{1}$$

$$\hat{H}^0_{\rm el} = -t \sum_{\langle ij\rangle\sigma} \left(\hat{c}^\dagger_{i\sigma}\hat{c}_{j\sigma} + \hat{c}^\dagger_{j\sigma}\hat{c}_{i\sigma} \right) - \mu \sum_{i\sigma} \hat{n}_{i\sigma},$$

$$\hat{H}^0_{\rm ph} = \frac{1}{2}\,\omega_0^2 \sum_i \hat{x}_i^2 + \frac{1}{2}\sum_i \hat{p}_i^2 \ ,$$

$$\hat{V}_{\rm el-ph} = \lambda_0 \sum_{ir\sigma} f(r)\,\hat{x}_i\,\hat{n}_{i+r,\sigma}, \qquad f(r) = \frac{e^{-r/\xi}}{(1+r^2)^{3/2}}.$$

$\hat{c}^\dagger_{i\sigma}$ and $\hat{c}_{j\sigma}$ are creation and destruction operators for electrons of spin σ on lattice site i, so that $\hat{H}^0_{\rm el}$ describes the hopping of electrons of spin σ between near neighbor sites $\langle ij\rangle$. Here we focus on a 2D square lattice and choose $t = 1$ to set the energy scale. $\hat{H}^0_{\rm ph}$ represents a dispersionless (optical) phonon mode on each lattice site. In $\hat{V}_{\rm el-ph}$, the phonon displacement $\hat{x}_i$ on site i couples to the electron densities $\hat{n}_{i+r,\sigma}$ with a strength $\lambda_0 f(r)$ which falls off exponentially with separation r[23]. Our simulations are done in the grand-canonical ensemble, with a chemical potential μ which couples to the fermion density $\hat{n}_{i\sigma} = \hat{c}^\dagger_{i\sigma}\hat{c}_{i\sigma}$. When $\mu = -(\sum_r \lambda(r))^2/\omega_0^2$, the Hamiltonian is particle-hole symmetric which assures that $\langle \hat{n}_{i,\uparrow} + \hat{n}_{i,\downarrow}\rangle = 1$, *i.e.* the system is at half filling (on average). In the literature, $\hat{V}_{\rm el-ph}$ is sometimes written by replacing $\hat{x}_i \rightarrow (\hat{a}^\dagger_i + \hat{a}_i)/\sqrt{2\omega_0}$ and defining the coupling $g = \lambda_0/\sqrt{2\omega_0}$. We will use this notation in our work as well.

The Holstein model[24], which has been the focus of most of the previous QMC investigations, is obtained in the extreme short-range limit $\xi \rightarrow 0$ where the phonon mode on site i couples only to the electron density on the same site. Since the Holstein electron-phonon coupling is absolutely local in space, it has no momentum dependence. Equation 1, on the other hand, allows for (a specific) $\tilde{\lambda}(q)$ via the Fourier transform of $\lambda_0 f(r)$. Continuous Time Quantum Monte Carlo (CTQMC) has been used to study the effect of varying the range ξ on polaron and bipolaron formation[15]. A momentum averaging technique has also been developed to study general $\lambda(q)$[25].

The interest in studying momentum-dependent coupling is driven by a number of factors. First, a momentum dependent $\tilde{\lambda}(q)$ has been suggested to play a role in superconducting transitions in FeSe monolayers[26], electron-phonon physics in $SrTiO_3$[27], and the behavior of 2H-$NbSe_2$[28]. Second, there are qualitative issues to be addressed, *e.g.* how the range of the electron phonon interaction, ξ, affects the competition between metallic and Peierls/CDW phases at half-filling. Here, recent CTQMC studies in one dimension have shown that as ξ increases from zero, the metallic phase is stabilized and, for sufficiently large λ_0, phase separation can also occur[29]. Finally, it has been suggested that materials-specific forms for $\lambda(q)$ can be incorporated into QMC simulations of appropriate model Hamiltonians[30].

The solution of Eq.(1) via QMC proceeds as follows. The inverse temperature β is discretized into L_τ intervals of length $\Delta\tau \equiv \beta/L_\tau$. Complete sets of phonon variables $\{x(i,\tau), p(i,\tau)\}$ are introduced at each imaginary time slice of the partition function $\mathcal{Z} = {\rm Tr}\, e^{-\beta\hat{H}} = {\rm Tr}\, e^{-\Delta\tau\hat{H}} e^{-\Delta\tau\hat{H}} \cdots e^{-\Delta\tau\hat{H}}$. We integrate out the momentum and, since the Hamiltonian is quadratic in the fermionic operators, they can be traced out finally giving[16],

$$\mathcal{Z} = \int \mathcal{D}\,x(i,\tau)\ e^{-S_{\rm bose}} \left(\det M(\{x(i,\tau)\}\right)^2, \tag{2}$$

$$S_{\rm bose} = \frac{1}{2}\Delta\tau\omega^2 \sum_{i,\tau} x(i,\tau)^2 + \frac{1}{2}\Delta\tau \sum_{i,\tau} \left(\frac{x(i,\tau+1) - x(i,\tau)}{\Delta\tau} \right)^2,$$

is an integral over the space and imaginary time dependent scalar phonon field $x(i,\tau)$. The integrand has a "bosonic" piece, $S_{\rm bose}$, originating in $\hat{H}^0_{\rm ph}$ and *identical* fermion determinants (one for each spin species) arising from integrating out the fermions. The matrix elements of M depend on the phonon field. Details of the form of M are in Ref. [31]. This general approach, is often referred to as the "Determinant Quantum Monte Carlo" (DQMC) method[31,32].

DQMC can be applied to models with el-el (as opposed to el-ph) interactions like the Hubbard Hamiltonian via the introduction of a Hubbard-Stratonivich (HS) field which decouples the quartic interaction terms to quadratics, allowing the fermion trace to be performed as above. In such applications, there is typically a sign problem- the product $\det M_\uparrow(\{x(i,\tau)\})\ \det M_\downarrow(\{x(i,\tau)\})$ can become negative, precluding the sampling of the HS Field. A crucial observation for the electron-phonon model of Eq. 1 is that the up and down fermion matrices are identical (hence their spin index is suppressed in Eq. 2.), and there is no sign problem.

At this point there are two approaches. In almost

all CM applications, the determinant of M, which is a very sparse dimension $L_\tau N$ matrix, is rewritten as the determinant of a smaller, dense, dimension N matrix where N is the number of sites. Changes to the phonon field variables $x(i,\tau)$ are performed individually and, because of their local nature, the change in $\det M$ can be evaluated in $\mathcal{O}(1)$ operations if the Green function $G = M^{-1}$ is known. After each change, G must be updated, a process which takes $\mathcal{O}(N^2)$ steps, since the change to a single $x(i,\tau)$ involves only a rank one alteration of M. A sweep of all NL_τ variables then requires $\mathcal{O}(N^3 L_\tau)$ steps.

The second approach (used in the majority of LGT applications) retains the larger sparse matrix M as the central object. All degrees of freedom are updated simultaneously using the Langevin equation, in a manner that is linear in both N and L_τ, under the assumption that the sparse linear algebra solver does not have an iteration count which increases with system size. This assumption fails dramatically for the Hubbard model, where there is no $S_{\rm bose}$ for the HS field. We will explore here the efficacy of the Langevin approach for electron-phonon models. Many subtleties need to be carefully assessed to perform a meaningful comparison with the $\mathcal{O}(N^3 L_\tau)$ approach. First, for a choice of Hamiltonian parameters, the dependence of the iteration count on N and L_τ must be monitored. Second, the equilibration and autocorrelation times must be measured. At a minimum, the iteration count and correlation times provide a potentially large prefactor to the linear scaling, competing with the savings due to linear scaling as opposed to cubic scaling. Finally, the effect of the discretization of the Langevin evolution on physical observables must be determined. These issues must be well understood as a function of the parameters in the Hamiltonian (the location in phase space).

We now describe the details of our approach, which is based on the algorithm in Ref. [33]. We first write Eq. (2) in the form,

$$\mathcal{Z} = \int \mathcal{D}\, x(i,\tau)\; e^{-S}, \tag{3}$$

where

$$S = S_{\rm bose} - \ln(\det M)^2, \tag{4}$$

and define fictitious dynamics governed by the Langevin equation,

$$\frac{{\rm d}x(j,\tau,t)}{{\rm d}t} = -\frac{\partial S}{\partial x(j,\tau,t)} + \sqrt{2}\,\eta(j,\tau,t), \tag{5}$$

with the stochastic variable η satisfying

$$\langle \eta(j,\tau,t)\rangle = 0,\ \langle \eta(j,\tau,t)\eta(r,\tau',t')\rangle = \delta_{j,r}\delta_{\tau,\tau'}\delta(t-t'). \tag{6}$$

In Eqs. (5,6), j labels the spatial coordinate of a site, τ its imaginary time and t the Langevin time. The condition given by Eq. (6) can be satisfied by taking the stochastic variables η to be random numbers with Gaussian distribution. The stationary limit of the statistical weight of the configurations, $P(\{x(i,\tau)\})$, can be determined by first writing the Fokker-Planck equation associated with Eq. (5) which describes the time evolution of P. It can then be easily shown[33] that in the long time limit the distribution is given by $P = \exp(-S)$, justifying using Eq. (5) to generate configurations which are used to calculate physical quantities.

To integrate Eq. (5), we first discretize the Langevin time. The simplest, Euler, discretization leads to[33],

$$\begin{aligned} x(j,\tau,t+{\rm d}t) = x(j,\tau,t) - {\rm d}t\frac{\partial S}{\partial x(j,\tau,t)} \\ +\sqrt{2{\rm d}t}\,\eta(j,\tau,t), \end{aligned} \tag{7}$$

with

$$\begin{aligned} \langle \eta(j,\tau,t\rangle = 0, \\ \langle \eta(j,\tau,t)\eta(r,\tau',t')\rangle = \delta_{j,r'}\delta_{\tau,\tau'}\delta_{t,t'}. \end{aligned} \tag{8}$$

Note the square root of the Langevin time step, ${\rm d}t$, in Eq. (7) which comes from replacing the Dirac δ-function in Eq. (6) by the discrete Kronecker δ, $\delta(t-t') \to \delta_{t,t'}/{\rm d}t$. Because of this $\sqrt{{\rm d}t}$, the Euler discretization error of this stochastic differential equation is $\mathcal{O}({\rm d}t)$ (for ${\rm d}t$ small enough) instead of the $\mathcal{O}({\rm d}t^2)$ for deterministic differential equations. To reduce the error in Eq. (7) to $\mathcal{O}({\rm d}t^2)$, one can use Runge-Kutta discretizations adapted to stochastic differential equations[33]. However, in this work, we have found that the simple Euler discretization has sufficient precision.

Now we deal with the action term,

$$\begin{aligned} \frac{\partial S}{\partial x(j,\tau,t)} &= \frac{\partial S_{\rm bose}}{\partial x(j,\tau,t)} - \frac{\partial \ln(\det M)^2}{\partial x(j,\tau,t)}, \\ &= \frac{\partial S_{\rm bose}}{\partial x(j,\ell,t)} - 2\,{\rm Tr}\left(\frac{\partial M}{\partial x(j,\ell,t)}M^{-1}\right). \end{aligned} \tag{9}$$

The trace term in Eq. (9) is expensive due to M^{-1}; calculating the inverse of a matrix scales as the cube of its dimension. In order to avoid this, we note that, given a vector of Gaussian random numbers, $\vec{g}$, and a matrix A, we have $\langle\, \vec{g}^{\,T} A\, \vec{g}\,\rangle = {\rm Tr}A$ where the average is taken over the Gaussian distribution of the random numbers. This allows us to replace the trace term in Eq. (9) by a stochastic estimator,

$$2\,{\rm Tr}\left(\frac{\partial M}{\partial x(j,\ell,t)}M^{-1}\right) \Longrightarrow 2\,\vec{g}^{\,T}\left(\frac{\partial M}{\partial x(j,\ell,t)}M^{-1}\right)\vec{g}. \tag{10}$$

We recall here that we are using the large sparse form of the matrix M, *i.e.* a sparse matrix with dimension NL_τ. Consequently, $\vec{g}$ is a vector with NL_τ elements. Using this estimator, we avoid having to calculate M^{-1} because what is needed now is $M^{-1}\vec{g}$, which is much faster to evaluate using, for example, the bi-Conjugate Gradient (CG) algorithm to solve $M\vec{v} = \vec{g}$. For a positive matrix, CG is guaranteed to converge to the exact result in at most NL_τ iterations. The issue of the positivity of

M is a subtle one which we shall not address here[1–4]. Of course, one does not need the exact answer and, instead, sets a precision threshold at which the CG iterations are stopped. Usually this leads to a rather small number of iterations (see below).

The Langevin iterations are implemented using Eqs. (7,6) with

$$\frac{\partial S}{\partial x(j,\tau,t)} = \frac{\partial S_{\rm bose}}{\partial x(j,\tau,t)} - 2\vec{g}^{\,T}\left(\frac{\partial M}{\partial \phi(\mathbf{j},\ell,t)}M^{-1}\right)\vec{g}. \quad (11)$$

Note that in this algorithm, the entire phonon field, $x(j,\tau)$, is updated in a single step. All the operations are simple sparse matrix-vector multiplies which can be easily optimized.

One of the main problems, mentioned earlier, facing simulations of electron-phonon systems is the very long auto-correlation times. We introduce Fourier acceleration (FA) which helps reduce this problem. We first note that Eq. (5) is just one in an infinite class of Langevin equations, all of which lead to the same stationary limit. Consider an arbitrary but positive definite matrix Q. Configurations generated by the Langevin equation,

$$\frac{{\rm d}\vec{x}(t)}{{\rm d}t} = -Q\frac{{\rm d}S}{{\rm d}\vec{x}(t)} + \sqrt{2Q}\,\vec{\eta}(t), \quad (12)$$

are guaranteed to be given by the correct distribution $(\exp(-S))$ in the long time limit regardless of the form of Q. This additional flexibility offers the possibility of choosing Q to shorten autocorrelation times, leading to accelerated convergence. To guide our choice, we note that in the noninteracting limit, $\lambda_0 = 0$, we have,

$$\frac{{\rm d}S}{{\rm d}x(i,\tau)} = \Delta\tau\,\omega^2 x(i,\tau) + \frac{[x(i,\tau+1)+x(i,\tau-1)-2x(i,\tau)]}{\Delta\tau}, \quad (13)$$

which becomes, after Fourier transforming along imaginary time,

$$\frac{{\rm d}\tilde{S}}{{\rm d}\tilde{x}(i,k_\tau)} = \left(\Delta\tau\,\omega_0^2 + [2-2\cos(2\pi k_\tau/L_\tau)]/\Delta\tau\right)\tilde{x}(i,k_\tau), \quad (14)$$

with $-L_\tau/2+1 \le k_\tau \le L_\tau/2$. We see that the ratio of the slowest to fastest mode is,

$$\frac{(\Delta\tau\,\omega_0)^2}{4+(\Delta\tau\,\omega_0)^2} \ll 1, \quad (15)$$

exposing the critical slowing down of the phonons in the imaginary time direction, especially at small $\Delta\tau$. To compensate for this, we choose the matrix Q to be diagonal in imaginary time Fourier space and given by,

$$\tilde{Q}(k_\tau) = \frac{\Delta\tau\omega_0^2 + 4/\Delta\tau}{\Delta\tau\omega_0^2 + (2-2\cos(2\pi k_\tau/L_\tau))/\Delta\tau}, \quad (16)$$

which is normalized so that $\tilde{Q}(L_\tau/2) = 1$. In the noninteracting limit, this choice will totally eliminate critical slowing down. This is clearly not true when $\lambda_0 \neq 0$. Nonetheless we find that this form, motivated by the noninteracting limit, works very well and helps convergence even in the strongly interacting case. We, therefore, use this form in all the follows.

Our Langevin equation now becomes,

$$\begin{aligned}\frac{{\rm d}\vec{x}(t)}{{\rm d}t} &= -\hat{\mathbf{F}}^{-1}\tilde{Q}(k_\tau)\hat{\mathbf{F}}\frac{{\rm d}S}{{\rm d}\vec{x}(t)} + \hat{\mathbf{F}}^{-1}\sqrt{2\tilde{Q}(k_\tau)}\,\hat{\mathbf{F}}\vec{\eta}(t) \\ &= -\hat{\mathbf{F}}^{-1}\left[\tilde{Q}(k_\tau)\hat{\mathbf{F}}\frac{{\rm d}S}{{\rm d}\vec{x}(t)} + \sqrt{2\tilde{Q}(k_\tau)}\,\hat{\mathbf{F}}\vec{\eta}(t)\right], \quad (17)\end{aligned}$$

where $\hat{\mathbf{F}}$ is an FFT operator, $\tilde{Q}(k_\tau)$ is given by Eq. (16), and ${\rm d}S/{\rm d}\vec{x}$ is given by Eq. (11).

Calculating phonon quantities is straight forward since the QMC evolves the phonon field directly. All fermioinc quantities can be calculated once the Green function is obtained. This is given by,

$$G(i,j) = \left\langle (M[\{x\}])^{-1}_{i,j}\right\rangle, \quad (18)$$

where the sites i and j can be at equal or unequal imaginary time. (Indeed, an additional advantage of the Langevin approach is that one does not need separate, and computationally costly, routines to evaluate the unequal time Green function.) As we did in the update steps, we avoid evaluating the inverse of the matrix M by calculating the Green function using a stochastic estimator,

$$G(i,j) = \left\langle \gamma_i \left(M[\{x\}]^{-1}\vec{\gamma}\right)_j\right\rangle, \quad (19)$$

where γ_j is a Gaussian random number. $M^{-1}\vec{\gamma}$ is calculated with the CG algorithm. Once $G(i,j)$ is calculated, all fermionic quantities, *e.g.* kinetic energy, density correlations, structure factor etc, can be obtained.

Long range CDW order is identified by studying $S(\pi,\pi)$ where the structure factor is given by

$$S(k_x,k_y) = \frac{1}{N}\sum_{\vec{r}} {\rm e}^{i\vec{k}\cdot\vec{r}}\langle n(0)n(\vec{r})\rangle. \quad (20)$$

III. BENCHMARKING THE ALGORITHM

We begin by addressing the first of the two themes of this paper: an investigation of algorithmic efficiency of Langevin-based linear scaling (iterative) methods in electron-phonon models.

Figure 1 shows the of CPU time for the Langevin and DQMC algorithms as a function of system size $N = L_x \times L_y$ at phonon frequency $\omega_0 = 2$, electron phonon coupling $g = 1$ and $\xi \to 0$ (*i.e.* the Holstein contact interaction limit). The chemical potential $\mu = -1$ is set so that

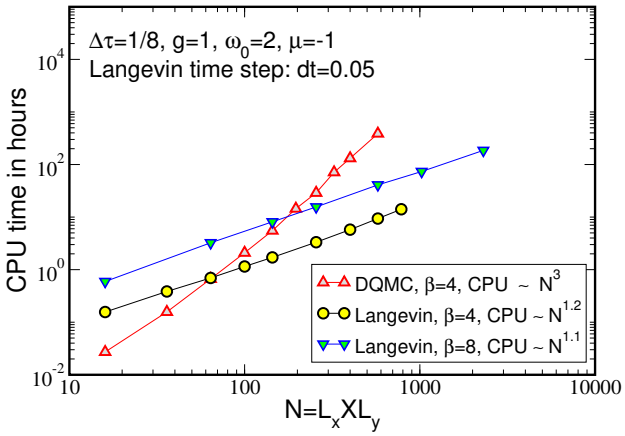

FIG. 1. (Color online) CPU time versus system size in the Holstein limit ($\xi \to 0$) for DQMC and Langevin algorithms. DQMC scales as N^3 while Langevin scales essentially linearly for both values of β. $\lambda_0 = g\sqrt{2\omega_0}$.

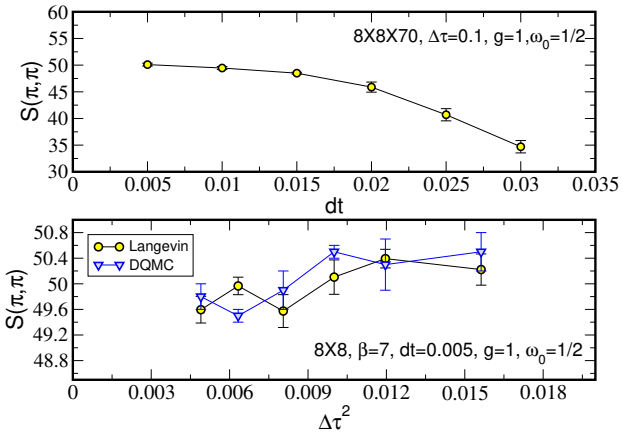

FIG. 2. (Color online) Top: The dependence of $S(\pi,\pi)$ on the Langevin time step, dt in the ordered phase. For d$t \leq 0.01$ the discretization error becomes linear in dt. Bottom: The dependence of $S(\pi,\pi)$ on the imaginary time step, $\Delta\tau$, for both DQMC and Langevin. The Trotter-Suzuki errors are comparable in the two algorithms. d$t = 0.005$ used to integrate the Langevin equation gives excellent agreement with DQMC. The data are for the Holstein limit ($\xi \to 0$).

the lattice is half-filled, $\rho = 1$. For this figure, the same number of sweeps was chosen for all the DQMC sizes, and a different fixed number of sweeps for the Langevin runs. The goal is simply to show the scaling of CPU time.

The log-log plot demonstrates the expected N^3 scaling for DQMC, and a near-linear scaling for the Langevin approach. That the power is slightly larger than one is a consequence of a modest increase in the number of conjugate gradient iterations with N. The Langevin approach already becomes more efficient than DQMC for relatively small lattice sizes, $N \sim 8 \times 8$ for $\beta = 4$. A key feature of Fig. 1 is that the (near) linear scaling is no worse at $\beta = 8$ than at $\beta = 4$. In contrast, in simulations of the Hubbard model, the number of conjugate gradient iterations grows very rapidly at large β and strong coupling U.

Figure 2 addresses the systematic errors in the Langevin approach. In the top panel, the charge density structure factor is shown as a function of Langevin step dt. The lattice size is $N = 8 \times 8$ and the inverse temperature $\beta = 7$ (deep in the ordered phase) with $\Delta\tau = 0.1$. It is seen that for dt less than around 0.015, the value of the structure factor changes very little and, in fact, the error varies linearly with dt. For d$t > 0.015$, the error increases rapidly until the iterative process is destabilized beyond d$t \approx 0.3$ for the parameters dshown in the figure. In the bottom panel the Trotter errors are assessed at fixed Langevin step d$t = 0.005$ and compared with those arising from DQMC. They are seen to be less than one percent up to $\Delta\tau^2 = 0.016$ ($\Delta\tau = 0.125$), and are comparable for the two methods.

Equilibration and autocorrelation times play a key role in the assessment of any algorithm. Figure 3 shows the equilibration of the charge density structure factor

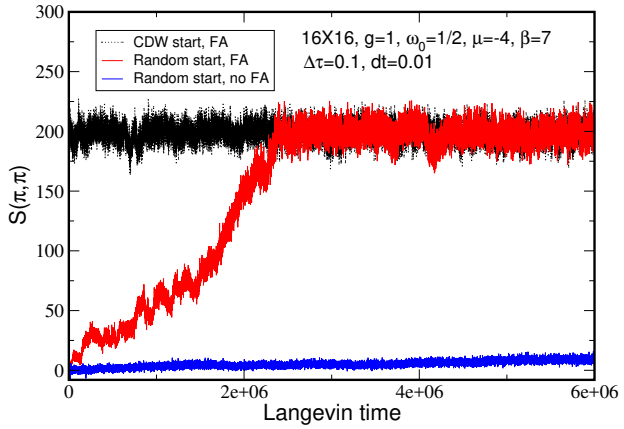

FIG. 3. (Color online) $S(\pi,\pi)$ as a function of Langevin time, comparing Fourier acceleration (FA) with unaccelerated evolution. The red (FA) and blue (no FA) curves have the same random initial configuration of the phonon field. It is clear that for large systems FA is crucial for equilibration. The initial configuration for the black curve is CDW: The phonon field has an initial checkerboard configuration.

$S(\pi,\pi)$ on a $N = 16 \times 16$ lattice at $\beta = 7$ with $\omega_0 = 0.5$, $g = 1$ ($\lambda_0 = 1$) and $\xi \to 0$. The lattice is half-filled ($\mu = -4$). In the absence of Fourier Acceleration, and with a random start, the system remains in the disordered state ($S(\pi,\pi)$ small) even out to six million

time steps. On the other hand, if FA is implemented, it grows steadily, achieving a value consistent with the known CDW order at $t \sim 2 \times 10^6$. If the simulation is started in a CDW pattern, it remains in that phase.

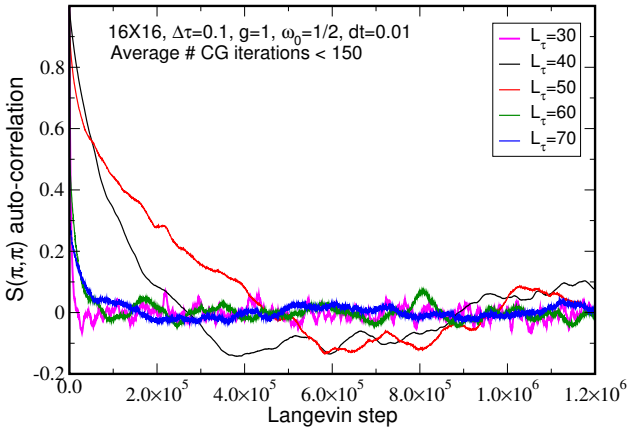

FIG. 4. (Color online) The autocorrelation function of accelerated Langevin dynamics of the Holstein model for several β values. The relaxation time is longest for $L_\tau = 40,\ 50$ ($\beta = 4,\ 5$) near the critical temperature, $\beta \approx 4.5$.

Figure 4 shows the autocorrelation function in the presence of FA for a $N = 16 \times 16$ lattice. Deep in the CDW phase, $L_\tau = 60, 70$ ($\beta = 6, 7$), as well as in the high temperature phase, $L_\tau = 30$ ($\beta = 3$) the autocorrelation time is relatively short. As is typical, autocorrelation times are long near the critical $\beta_c \sim 4.5$ as seen from the data with $L_\tau = 40, 50$ ($\beta = 4, 5$).

IV. THE PHASE DIAGRAM OF THE LONG RANGE MODEL

We focus in this paper on a longer range el-ph coupling given by Eq. 1. Several initial efforts have been made to study this situation[35,36]. They have found a significant tendency to phase separation. The qualitative physics behind this is clear: In the Holstein model an electron of one spin distorts the phonon on its same site, attracting an electron of opposite spin there. The Pauli principle precludes any further clustering. If, however, the interaction extends to neighboring sites, electrons will get attracted there. These, in turn will bring in yet more particles on next-near neighbor sites. This cascading effect costs kinetic energy, and entropy, but still might dominate the physics. It has proven difficult to expose the extent of phase separation in traditional DQMC algorithms, since the longer range interaction makes the update of the Green function more expensive. At minimum there is a succession of rank one updates whose number equals the number of sites within the interaction range. If ξ is large enough, the expense goes from $\mathcal{O}(N^3)$ to $\mathcal{O}(N^4)$.

Our specific goal is to get the ground state phase diagram in the $\lambda_0 - \xi$ plane. We begin by studying the real space density-density correlation function and its Fourier transform, the CDW structure factor, Eq.(20). In the disordered phase, $S(\pi, \pi)$ picks up contributions only from a small number of terms, while in the ordered phase, $S(\pi, \pi)$ will grow linearly with N.

Figure 5 shows $S(\pi, \pi)/N$ for several lattice sizes N as a function of ξ at fixed $\beta = 9.6$, $\omega_0 = 0.5$ and $\lambda_0 = 1.5$. Data for different N coincide at small ξ, indicating long range order. At $\xi \approx 0.4$, $S(\pi, \pi)$ falls rapidly. This parameter sweep represents one cut through the phase diagram of Fig. 11. We have also verified that the single particle Green function, Eq.(18), and the pair correlation function, $\langle \Delta_i^\dagger \Delta_j \rangle$ with $\Delta_i \equiv c_\uparrow(i) c_\downarrow(i)$, both decay exponentially with $|i - j|$ in the CDW phase. This confirms that the system is in an insulating phase.

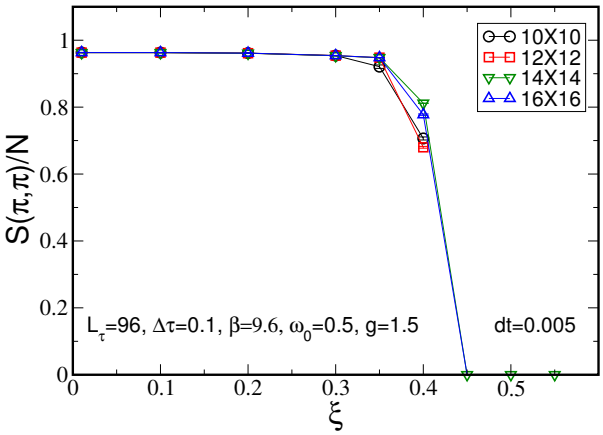

FIG. 5. (Color online) The structure factor, $S(\pi, \pi)$ as a function of the range of the interaction, ξ, keeping the chemical potential tuned to half filling. When the interaction is large enough, $S(\pi, \pi)$ drops to zero due to phase separation. See the phase diagram of Fig. 11.

Figure 6, which shows the density for the same parameters as Fig. 5, suggests the collapse of CDW order is not due to the density-density correlator becoming random (as would occur if one heats the Holstein model above its T_c). Instead, the particle density plummets although the chemical potential is chosen to yield half filling. This suggests phase separation as ξ grows.

Figure 7 shows results in which instead λ_0 is increased at fixed $\xi = 0.5$. Large density fluctuations set in at $\lambda_0 \gtrsim 0.7$, again indicating phase separation. This provides another cut in the λ_0-ξ plane to generate the phase boundary of Fig. 11.

Fixing $\xi = 0.2$, $S(\pi, \pi)$ grows rapidly at $\lambda_0 \sim 0.6$ for $\beta = 9.6$ (Fig. 8). We believe that the region of small

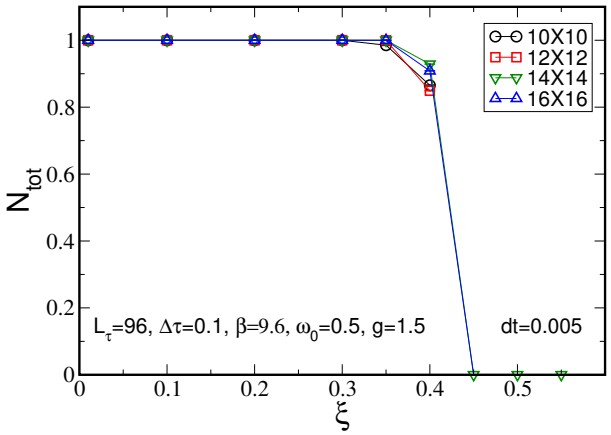

FIG. 6. (Color online) Same as Fig. 5 but showing the total number of particles. For $\xi \gtrsim 0.4$ the occupation vanishes, indicating phase separation. See Fig. 11.

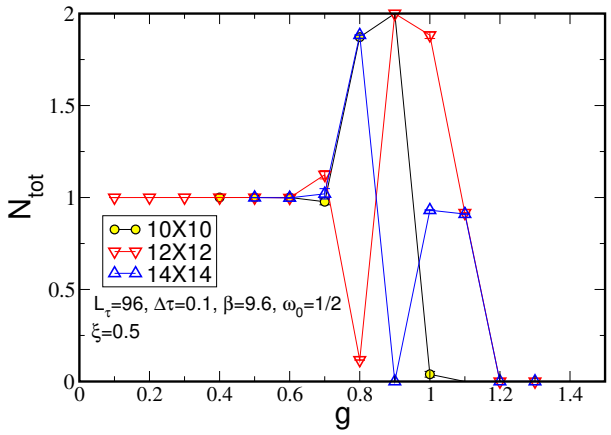

FIG. 7. (Color online) The total occupation as a function of the interaction strength at fixed (large) ξ. For $\lambda_0 > 0.7$ the system is either empty or totally full, indicating phase separation. See Fig. 11.

$S(\pi,\pi)$, $\lambda_0 \lesssim 0.6$, is associated with the fact that the transition temperature is exponentially low. We see no evidence for phase separation. This is also confirmed in Fig. 9 where one sees a growth of $S(\pi,\pi)$ in the small λ region as T is lowered. The observation of ordered phases at weak coupling is often a subtle issue in finite temperature simulations, since, for example, one often has BCS-like functional forms $T_c \sim \omega e^{-ct/\lambda}$ which become exponentially small as λ decreases. This is supported by the fact that $S(\pi,\pi)$ grows as β increases, unlike situations where there is a disordered phase below a critical coupling value, as occurs on a honeycomb lattice[37,38].

The difficulty in observing the CDW phase, at small g and finite temperature, was also noted for the Holstein model ($\xi = 0$) in Ref. 19, which presented QMC results and arguments supporting the existence of the CDW phase down to very small values of g with the possibility of zero temperature transition. On the other hand, Ref. 20 used variational MC to argue that, for small interaction, the system has either a paramagnetic or a weak superconducting phase. Reference 21, also using variational MC, argued that for small values of the interaction the system is superconducting. So, the situation at weak interaction is not settled for $\xi = 0$. For $\xi \neq 0$, we had the same difficulties for small g, and it is natural to suppose that this is due to the same reasons as $\xi = 0$. Of course for $g = 0$ and any ξ the system is a simple metal.

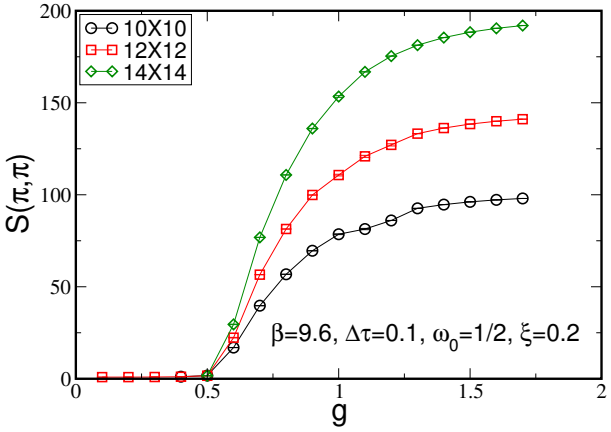

FIG. 8. (Color online) $S(\pi,\pi)$ as a function of λ_0 at fixed $\xi = 0.2$ where there is no phase separation (See Fig. 11). As λ_0 decreases, $S(\pi,\pi)$ decreases, becoming small for $\lambda_0 < 0.4$. We believe this is due to an exponentially small T_c which has decreased below our simulation temperatures $T \sim (1/16 - 1/64)\, t$ rather than a lack of CDW order. See text.

Although we have focused on the (momentum space) CDW structure factor, one can also of course observe the oscillating density correlations directly in real space. An example is given in Fig. 10. At fixed $\beta = 9.6$ and $g = 1.0$, robust density oscillations occur up to $\xi = 0.3$. For $\xi = 0.4$ the system has undergone phase separation and the density correlation function no longer exhibits CDW oscillations.

Taken together, Figs. 5-10 can be used to generate the phase diagram at $\beta = 9.6$ shown in Fig. 11. The entire region below the dashed (red) line is where we cannot, at the moment, characterize the phase unambiguously. Based on various results, this region can be CDW, superconducting or paramagnetic (see the discussion above). Note that for the one-dimensional system, the

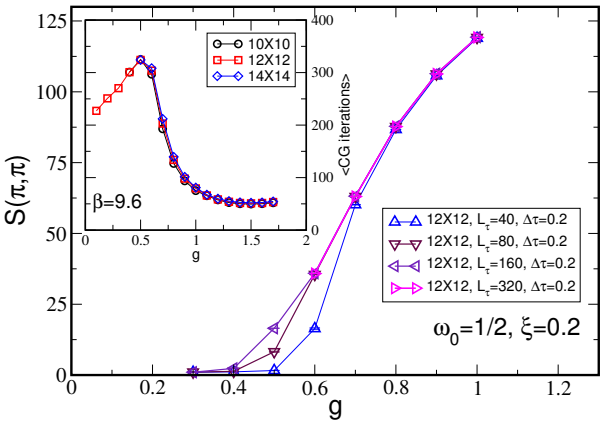

FIG. 9. (Color online) Same as Fig. 8 but for one size and several values of β. $S(\pi,\pi)$ increases, and then saturates, as β is increased. We are unable to see the CDW phase unambiguously for $\lambda_0 < 0.4$. Inset: For the same ω_0 and ξ and for $\beta = 9.6$, we show the average number of CG iterations as a function of the coupling g. At weak coupling, the number of iterations is large, peaks at $g = 0.5$, and decreases rapidly as the CDW gap strengthens. Note the absence of dependence on system size.

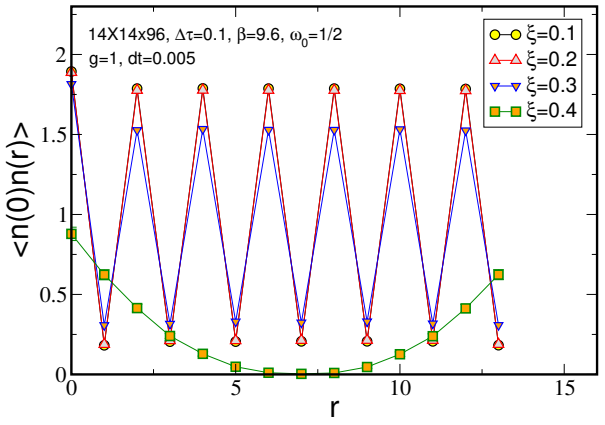

FIG. 10. (Color online) The density correlation function as a function of distance at fixed $g = 1$ and $\xi = 0.1$, 0.2, 0.3, 0.4. For the first three values of ξ, the system is in the CDW phase, as is clear from the robust oscillation of the correlation function. For $\xi = 0.4$ the system has undergone phase separation.

small g region corresponds to a metallic phase[29].

Figure 11 shows the phase diagram at very low temperature. Since CDW formation breaks a discrete symmetry, we expect that in two dimensions the phase transition occurs at finite critical temperarture,

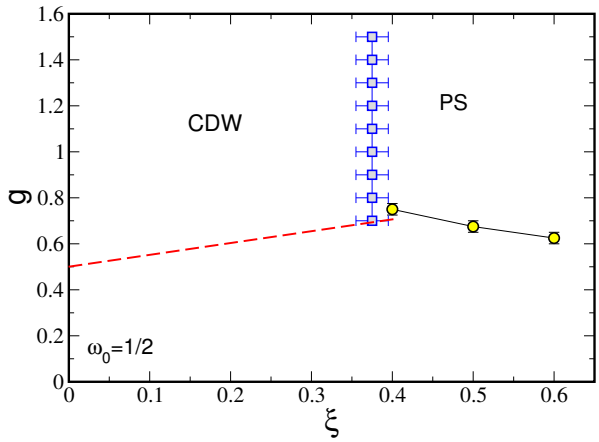

FIG. 11. (Color online) The phase diagram in the g-ξ plane at half-filling and constant $\beta = 9.6$. The phonon frequency is fixed at $\omega = 1/2$. For $\xi = 0$, we have the Holstein model; for $g = 0$ and any ξ, the system is a simple metal. The nature of the phase below the dashed (red) line is not yet settled (see text).

T_c. This is confirmed in Fig. 12, for the Holstein model ($\xi = 0$), which shows a finite size scaling analysis of $S(\pi,\pi)$, making use of the expected Ising critical exponents[16,17,19]. The top panel uses data from the 'traditional' DQMC approach which is based on single phonon field updates and scales as $\mathcal{O}(N^3)$, while the bottom panel shows the Langevin results with computation time scaling linearly with N. The ability to simulate larger lattice sizes is seen to provide a more convincing data collapse, which occurs as the thermodynamic limit is approached. In addition, the efficiency of the algorithm allows us to get more precise results in reasonable computation time. As a benchmark, we note that the simulations of the 12×12 system took about 30% less time with the Langevin algorithm than with DQMC, and with error bars which are about half the size. For larger systems sizes, the run time difference favors Langevin even more because of the linear scaling as opposed to cubic for DQMC. We note that $\beta_c = 5.75(5)$ from the Langevin simulations and $\beta_c = 6.0(1)$ from DQMC. We believe this difference is due to the fact that DQMC experiences severe critical slowing down which the global updates relieve only partially while, on the other hand, Fourier acceleration in the Langevin algorithm is exceptionally efficient near critical points. In addition, much larger sizes were accessible with the Langevin algorithm than with DQMC, which makes the finite size scaling more reliable.

We performed such finite size scaling to find the critical inverse temparature, $\beta_c(\xi)$, as ξ is increased. Figure 13 shows the resulting phase diagram in the (ξ, β_c) plane illustrating that as ξ increases, β_c increases rapidly until

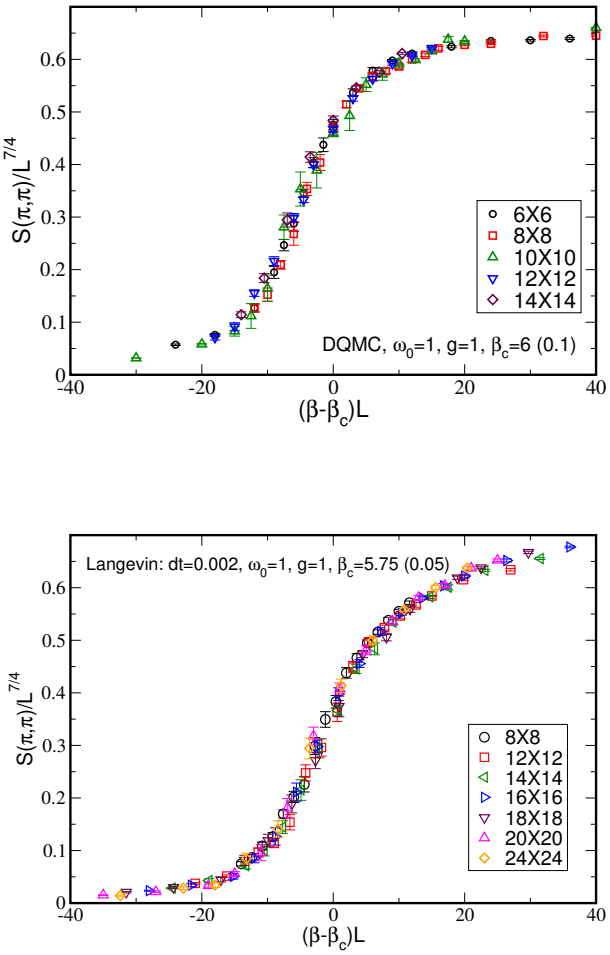

FIG. 12. (Color online) Scaling of the structure factor for the Holstein model ($\xi = 0$) near the finite temperature transition from disordered to CDW phase[22]. The top (bottom) panel shows DQMC (Langevin). Note the larger system sizes and the cleaner collapse in the Langevin case. We also note the small difference in β_c. between DQMC and Langevin (see text).

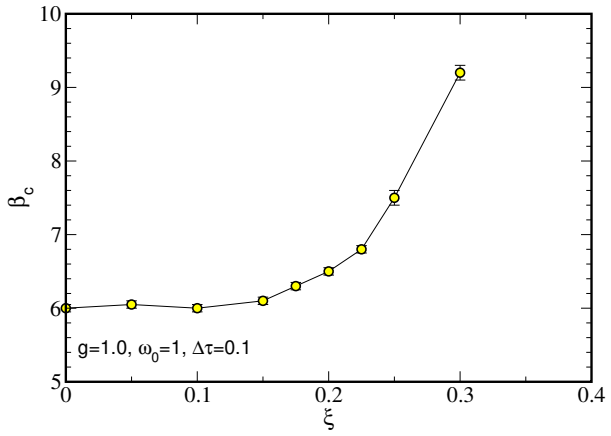

FIG. 13. (Color online) The critical inverse temperature, β_c, as a function of the range of the electron-phonon interaction, ξ. β_c was obtained by performing finite size scaling analysis as in Fig. 12.

phase separation occurs at large enough $\xi_c \approx 0.55$. We did not determine β_c beyond $\xi = 0.3$ since it becomes very large.

V. CONCLUSIONS AND OUTLOOK

In this paper we have formulated a Langevin-based Quantum Monte Carlo algorithm for an interacting electron-phonon Hamiltonian, augmented by Fourier Acceleration. Variation of the phonon field in the imaginary time direction is moderated by the phonon kinetic energy. As a consequence, the rapid growth in the number of conjugate gradient iterations needed in such approaches to the Hubbard model is not present here.

We have presented tests of our method which quantify various systematic errors. Comparisons with single update $\mathcal{O}(N^3)$ simulations using DQMC show that the Langevin method gives physically correct results, and also indicate that the cross-over where it becomes more efficient occurs at lattice sizes $N \sim 10^2$.

We have applied the method to an electron-phonon model with finite range (*i.e.* momentum-dependent) interaction. This is a natural target, since single update algorithms scale as $\mathcal{O}(N^4)$ and hence have proven extremely challenging. The phase diagram obtained indicates a strong tendency towards phase separation, even with correlation lengths as small as $\xi \sim 0.35$, a situation in which the near-neighbor coupling is nearly two orders of magnitude smaller than the on-site interaction.

This sensitivity to finite ξ suggests that application of such models to materials with momentum-dependent $\tilde{\lambda}(q)$ will need to include some sort of electron-electron interaction to inhibit phase separation. This is a very challenging task owing to the resulting sign problem of doped systems which would lead to a complex Langevin. Such equations have been studied quite extensively in the context LGT[39] and recently applied to the one dimensional Hubbard model[40] and ultra-cold fermionic atoms with unequal masses[41]. The complex Langevin equation was also recently applied to the Holstein-Hubbard model[42] and shown to be very efficient in the parameter range $U > g^2/\omega_0$.

More direct applications of our approach will be to the on-site (Holstein) case, for which there is still an abundance of open questions, including studies of 3D and layered 2D systems, accurate determination of critical

properties via finite size scaling, role of anharmonicities, and high resolution of observables in momentum space, all of which require large lattice sizes. In addition, SSH models where the hopping parameter fluctuates due to the nuclear oscillations can be treated efficiently with this algorithm. An interesting question to address is the competition between the contact Holstein coupling and the bond SSH coupling in determing the phase of the system. Finally, we note that, although in this paper we dealt only with the half-filled case, our method can be also applied to doped systems because the up and down fermion determinants are identical and, consequently, there is no fermion sign problem at any filling. In addition, as mentioned previously, space and time separated correlation functions can be calculated (see just after Eq.(18)) giving access to dynamic properties via maximum entropy.

VI. ACKNOWLEDGEMENTS

The work of RTS was supported by DOE-SC0014671. GGB is supported by the French government, through the UCAJEDI Investments in the Future project managed by the National Research Agency (ANR) with the reference number ANR-15-IDEX-01. We thank Steven Johnston, WeiTing Chiu, and Thomas Devereaux for useful conversations.

[1] "A New Algorithm for the Numerical Simulation of Fermions", R.T. Scalettar, D.J. Scalapino, and R.L. Sugar, Phys. Rev. B34, 7911 (1986).
[2] "A Hybrid-Molecular Dynamics Algorithm for the Numerical Simulation of Many Electron Systems", R.T. Scalettar, D.J. Scalapino, R.L. Sugar, and D. Toussaint, Phys. Rev. B36, 8632 (1987).
[3] "A High Quality Preconditioning Technique for Multi-Length-Scale Symmetric Positive Definite Linear Systems", I. Yamazaki, Z. Bai, W. Chen, and R. Scalettar, Numerical Mathematics: Theory, Methods and Applications **2**, 469 (2009).
[4] "Numerical Methods for Quantum Monte Carlo Simulations of the Hubbard Model", Zhaojun Bai, Wenbin Chen, Richard Scalettar and Ichitaro Yamazaki, in "Multi-Scale Phenomena in Complex Fluids" edited by Thomas Y. Hou, Chun Liu and Jian-Guo Liu, pp. 1-110, Higher Education Press (2009).
[5] "Revisiting the hybrid quantum Monte Carlo method for Hubbard and electron-phonon models", Stefan Beyl, Florian Goth, and Fakher F. Assaad Phys. Rev. B97, 085144 (2018).
[6] "Continuous-Time Quantum Monte Carlo Algorithm for the Lattice Polaron", P.E. Kornilovitch, Phys. Rev. Lett. 81, 5382 (1998).
[7] "Ground-state dispersion and density of states from path-integral Monte Carlo: Application to the lattice polaron", P.E. Kornilovitch, Phys. Rev. B60, 3237 (1999).
[8] "Polaron dynamics and bipolaron condensation in cuprates", A. S. Alexandrov, Phys. Rev. B61, 12315 (2000).
[9] "Quantum Monte Carlo and variational approaches to the Holstein model", M. Hohenadler, H. G. Evertz, and W. von der Linden, Phys. Rev. B69, 024301 (2004).
[10] "Dimensionality effects on the Holstein polaron", L.-C. Ku, S.A. Trugman, and J. Bonca, Phys. Rev. B65, 174306 (2002).
[11] "Effect of electron-phonon interaction range on lattice polaron dynamics: A continuous-time quantum Monte Carlo study", P.E. Spencer, J.H. Samson, P.E. Kornilovitch, and A.S. Alexandrov, Phys. Rev. B71, 184310 (2005).
[12] "Two dimensional Hubbard-Holstein bipolaron", A. Macridin, G.A. Sawatzky, and M. Jarrell, Phys. Rev. B69, 245111 (2004).
[13] "Effects of dimensionality and anisotropy on the Holstein polaron", A.H. Romero, D.W. Brown, and K. Lindenberg, Phys. Rev. B60, 14080 (1999).
[14] "Holstein polaron", J. Bonća, S.A. Trugman, and I. Batistić, Phys. Rev. B60, 1633 (1999).
[15] "Bipolarons from long-range interactions: Singlet and triplet pairs in the screened Hubbard-Fröhlich model on the chain", J.P. Hague and P.E. Kornilovitch, Phys. Rev. B80, 054301 (2009).
[16] "Competition of Pairing and Peierls–CDW Correlations in a 2–D Electron–Phonon Model", R.T. Scalettar, D.J. Scalapino, and N.E. Bickers, Phys. Rev. B40, 197 (1989).
[17] "CDW and Pairing Susceptibilities in a Two Dimensional Electron–Phonon Model", R.M. Noack, D.J. Scalapino, and R.T. Scalettar, Phys. Rev. Lett. 66, 778 (1991).
[18] "Charge Density Wave Gap Formation in the 2–dimensional Holstein Model at Half–Filling", P. Niyaz, J.E. Gubernatis, R.T. Scalettar, and C. Y. Fong, Phys. Rev. B48, 16011 (1993).
[19] "Two-Dimensional Holstein Model: Critical Temperature, Ising Universality, and Bipolaron Liquid", M. Weber and M. Hohenadler, Phys. Rev. B 98, 085405 (2018).
[20] "Competition among Superconducting, Antiferromagnetic, and Charge Orders with Intervention by Phase Separation in the 2D Holstein-Hubbard Model", T. Ohgoe and M. Imada, Phys. Rev. Lett. 119, 197001.
[21] "Superconductivity, charge-density waves, antiferromagnetism, and phase separation in the Hubbard-Holstein model", S. Karakuzu, L. F. Tocchio, S. Sorella, and F. Becca, Phys. Rev. B 96, 205145.
[22] "Phonon dispersion and the competition between pairing and charge order", N.C. Costa, T. Blommel. W.-T. Chiu, G.G. Batrouni, and R.T. Scalettar, Phys. Rev. Lett. 120, 187003.
[23] "Electrons in Lattice Fields", H. Fröhlich, Adv. Phys. 3, 325 (1954).
[24] "Studies of Polaron Motion 1. The Molecular-Crystal Model", T. Holstein, Ann. Phys. N.Y. 8, 325 (1959).
[25] "Momentum average approximation for models with electron-phonon coupling dependent on the phonon momentum", G.L. Goodvin and M. Berciu, Phys. Rev. B78, 235120 (2008).

[26] "Aspects of electron-phonon interactions with strong forward scattering in FeSe Thin Films on SrTiO 3 substrates", Y. Wang, K. Nakatsukasa, L. Rademaker, T. Berlijn, and S. Johnston, arXiv:1602.00656.
[27] "Strong polaronic behavior in a weak coupling superconductor", A.G. Swartz, H. Inoue, T.A. Merz, Y. Hikita, S. Raghu, T.P. Devereaux, S. Johnston, and H.Y. Hwang, arXiv:1608.05621.
[28] "Extended Phonon Collapse and the Origin of the Charge-Density Wave in 2H-NbSe", F. Weber, S. Rosenkranz, J.-P. Castellan, R. Osborn, R. Hott, R. Heid, K.-P. Bohnen, T. Egami, A.H. Said, and D. Reznik, Phys. Rev. Lett. 107, 107403 (2011).
[29] "Effect of Electron-Phonon Interaction Range for a Half-Filled Band in One Dimension", M. Hohenadler, F.F. Assaad, and H. Fehske, Phys. Rev. Lett. 109, 116407 (2012).
[30] "Directly characterizing the relative strength and momentum dependence of electron-phonon coupling using resonant inelastic x-ray scattering", T.P. Devereaux, A.M. Shvaika, K. Wu, K. Wohlfeld, C.J. Jia, Y. Wang, B. Moritz, L. Chaix, W.-S. Lee, Z.-X. Shen, G. Ghiringhelli, and L. Braicovich, arXiv 1605.03129.
[31] "Monte Carlo calculations of coupled boson-fermion systems. I", R. Blankenbecler, D.J. Scalapino, and R.L. Sugar, Phys. Rev. D24, 2278 (1981).
[32] "A Novel Technique for the Simulation of Interacting Fermion Systems", S. Sorella, S. Baroni, R. Car, and M. Parinello, Europhys. Lett. 8, 663 (1989).
[33] "Langevin Simulations of Lattice Field Theories", G. G. Batrouni, G. R. Katz, A. S. Kronfeld, G. P. Lepage, B. Svetitsky et K. G. Wilson, Physical Review D32, 2736 (1985).
[34] "Symmetry Enforced Self-Learning Monte Carlo Method Applied to the Holstein Model", Chuang Chen, Xiao Yan Xu, Junwei Liu, George Batrouni, Richard Scalettar and Zi Yang Meng, Phys. Rev. B98, 041102 (2018), rapid communication.
[35] S. Johnston, unpublished and private communication.
[36] T.P. Devereaux, unpublished and private communication.
[37] "Ground state and finite temperature signatures of quantum criticality in the Half-filled Hubbard Model on a Honeycomb Lattice", Thereza Paiva, R.T. Scalettar, W. Zheng, R.R.P. Singh, and J. Oitmaa, Phys. Rev. B72, 085123 (2005).
[38] Y.X. Zhang, W.T. Chiu, N.C. Costa, G.G. Batrouni, and R.T. Scalettar, unpublished.
[39] G. Aarts, E. Seiler, D. Sexty, and I-O, Stamatescu, 2017, *J. High Energ. Phys.* **44**.
[40] C. Loheac, and J. E. Drut, 2017, *Phys. Rev.* **D95**, 094502.
[41] L. Rammelmüller, J. E. Drut, and J. Braun, 2018, *J. Phys.: Conf. Ser.* **1041** 012006.
[42] S. Karakuzu, K. Seki, and S. Sorella, arXiv:1808.07759.